Springer

Acta Mechanica Sinica

CrossMark click for updates

•RESEARCH PAPER•

Acta Mech. Sin., Vol. 38, 521344 (2022)
https://doi.org/10.1007/s10409-021-09018-x

Multi-parameter joint optimization for double-strip high-speed pantographs to improve pantograph-catenary interaction quality

Mengzhen Wu[1,2], Xianghong Xu[2*], Yongzhao Yan[2], Yi Luo[2], Sijun Huang[3], and Jianshan Wang[1*]

[1] *School of Mechanical Engineering, Tianjin University, Tianjin 300354, China;*
[2] *State Key Laboratory of Nonlinear Mechanics, Institute of Mechanics, Chinese Academy of Sciences, Beijing 100190, China;*
[3] *Beijing CRRC CED Railway Electric Tech Company Limited, Beijing 100176, China*

Received July 9, 2021; accepted July 27, 2021; published online January 20, 2022

The significant increase in speed of high-speed train will cause the dynamic contact force of the pantograph-catenary system to fluctuate more severely, which poses a challenge to the study of the pantograph-catenary relationship and the design of high-speed pantographs. Good pantograph-catenary coupling quality is the essential condition to ensure safe and efficient operation of high-speed train, stable and reliable current collection, and reduction in the wear of contact wires and pantograph contact strips. Among them, the dynamic parameters of high-speed pantographs are crucial to pantograph-catenary coupling quality. With the reduction of the standard deviation of the pantograph-catenary contact force as the optimization goal, multi-parameter joint optimization designs for the high-speed pantograph with two contact strips at multiple running speeds are proposed. Moreover, combining the sensitivity analysis at the optimal solutions, with the parameters and characteristics of in-service DSA380 high-speed pantograph, the optimization proposal of DSA380 was given.

High-speed pantograph, Pantograph-catenary interaction quality, Multi-parameter joint optimization

Citation: M. Wu, X. Xu, Y. Yan, Y. Luo, S. Huang, and J. Wang, Multi-parameter joint optimization for double-strip high-speed pantographs to improve pantograph-catenary interaction quality, Acta Mech. Sin. **38**, 521344 (2022), https://doi.org/10.1007/s10409-021-09018-x

1. Introduction

The significant increase in speed of high-speed train has placed higher demands on the relationship between the pantograph and catenary [1]. A good pantograph-catenary relationship is the essential condition to ensure the stable and reliable current collection of the train and the reduction in friction between the contact wires and pantograph strips. In actual measurement and simulation analysis, the mean value F_m and standard deviation σ of the contact force are used as the main evaluation indexes of the current collection quality [2-4].Among them, F_m represents the level of contact force between the carbon strips and the catenary. When the train speed v is higher than 200 km h^{-1} (AC), the range of F_m should be between $0.00047v^2 + 60$ and $0.00097v^2 + 70$; σ represents the fluctuation of the contact force, which should meet $\sigma \leq 0.3F_m$. The smaller the F_m is, the smaller the mechanical friction between the carbon stripes and the catenary is; the smaller the σ is, the smaller the fluctuation of the pantograph-catenary contact force is, and the better the pantograph-catenary contact performance is. Therefore, a good pantograph-catenary relationship requires that σ should be as small as possible under the premise of satisfying the requirement for F_m. In the research on pantograph-catenary dynamics optimization, the standard deviation of the contact force is used as the objective function. In recent years, researchers have focused on pantograph-catenary dynamics simulation to study the influences of the model parameters on the pantograph-catenary performance, and to provide a parameter optimization scheme for improving the pantograph-catenary coupling quality to meet the needs of high-

*Corresponding authors. E-mail addresses: xxh@lnm.imech.ac.cn (Xianghong Xu); wangjs@tju.edu.cn (Jianshan Wang)
Executive Editor: Lifeng Wang

speed train with a significant increase in speed.

Running speed and model parameters of the pantograph-catenary system have different degrees of effects on the sensitivity rating and optimization schemes of the model parameters, as well as on the optimization effects of pantograph-catenary performance. With the control variate method, Cho et al. [5] obtained the optimal pre-sags of the simple catenary at the running speed of 170 km h^{-1} and 220 km h^{-1}, respectively, and proposed that, the optimal pre-sag and the percentage reduction of the standard deviation of contact force after optimization are relevant to the running speed. Gregori et al. [6] took the standard deviation of contact force as the objective function and used the genetic algorithm to calculate the optimal pre-sag for simple catenary and stitched catenary systems in the speed range from 200 km h^{-1} to 320 km h^{-1}. They concluded that the type of catenary and running speed have remarkable influences on the optimal pre-sag and the height of the contact wire at dropper point. Combining Spearman rank correlation coefficient method and Sobol sensitivity analysis method, Zhang et al. [7] believed that, regarding the standard deviation of contact force, the sensitivity rating and optimization direction of the tension and linear mass of contact wire are different at the running speeds of 300 km h^{-1}, 400 km h^{-1}, and 500 km h^{-1}. Meanwhile, researchers conducted sensitivity analysis of pantograph dynamic parameters based on the control variate method. Pombo and Ambrósio [8] conducted research on a Faiveley CX pantograph and a stitched catenary system at the running speed of 300 km h^{-1}. The results showed that the decrease of the equivalent mass or the increase of the equivalent stiffness of the pan-head, the increase of the equivalent damping of the lower frame, would reduce the standard deviation of the contact force. Zhou and Zhang [9] conducted a study on a DSA250 pantograph and a simple catenary system at the running speed of 250 km h^{-1}. The results showed that, the decrease in equivalent stiffness of the pan-head or upper frame, the increase in the equivalent damping of the pan-head or upper frame, would decrease the standard deviation of the contact force. Wu et al. [10] conducted research on a DSA380 pantograph and a stitched catenary at a running speed of 350 km h^{-1}. It was found that the decrease of the equivalent mass of the pan-head or lower frame, the decrease of the equivalent stiffness of the pan-head or upper frame, the increase of equivalent damping of the pan-head, upper frame, or lower frame, would increase the coupling performance of the pantograph-catenary. The above studies showed that under different cases, the reduction percentages of contact force standard deviation corresponding to the optimal solutions of these pantograph dynamic parameters were different.

The effects of multi-parameter joint optimization for pantograph-catenary system are superior to single-parameter or less-parameter optimization. Gregori et al. [6] used the genetic algorithm to make a pantograph-catenary parameter optimization at a running speed of 300 km h^{-1}. When the design vector was the height of the contact wire at dropper points, the standard deviation of contact force after optimization was reduced by 56.5% and 36.6%, respectively, for simple catenary and stitched catenary system, which were far higher than 26.0% and 0% in single pre-sag optimization. Zhang et al. [7] took the decision vectors as the first two or three among the tension and linear mass of the contact wire, and messenger wire tension, the standard deviation of contact force after optimization were decreased by 48.9% and 57.1%, respectively, which was better than that of the single-parameter optimization with respect to the contact wire tension, which was 31.6%. Lee et al. [11] established a quadratic function of and the standard deviation of the contact force vs. five pantograph parameters. The optimization result showed that the standard deviation of contact force decreased by 8.6%. Ambrósio et al. [12] used the genetic algorithm to conduct an optimization of multiple parameters, i.e., the equivalent mass, stiffness, and damping of the pan-head, and concluded that the standard deviation of contact force decreased by 11.0%. Wang et al. [13] established a quadratic function of the standard deviation of contact force vs. the seven dynamic parameters of the DSA250 pantograph at the running speed of 162 km h^{-1}. The result suggested that the joint optimization of seven parameters resulted in the reduction of the standard deviation of contact force by 27.1%. Wu et al. [10] used the method of exhaustion to conduct optimization of the equivalent stiffness and damping of the pan-head for DSA380 pantograph at the running speed of 350 km h^{-1}. The solution of this dual-parameter optimization resulted in a reduction of 4.5% in the standard deviation of contact force and superior to the single parameter optimization by 0.2%.

In this paper, the equivalent mass of the pan-head was set according to the parameters of a typical in-service high-speed pantograph DSA380 with two contact stripes, while the constraints of the other 8 dynamics parameters were determined considering the feasibility of engineering design. Based on the dynamics simulation of the high-speed pantograph-catenary system, multi-parameter joint optimization designs of the double-strip high-speed pantograph at various running speeds were proposed with the optimization objective of reducing the standard deviation of the contact force. Moreover, the optimization proposal for the DSA380 pantograph was given.

2. Dynamic model of the pantograph-catenary system

2.1 Dynamic equations of the catenary

Ignoring the stagger and lateral motion of the catenary, a two-dimensional finite element model of the stitched catenary system was established (Fig. 1) [14,15].

In this model, since the lengths of the contact wire, the messenger wire, and the stitch wire are much larger than their cross-sectional sizes, the bending stress caused by bending deformation is much smaller than the tensile stress caused by the pretension, and the bending stress has little effect on the dynamic contact force at frequencies below 50 Hz [16,17]. Therefore, the model can be simplified as a slender rod model [18-21]. The dropper is a slender string that can only bear tension, subject to axial expansion and contraction. It can be simplified as a nonlinear spring having only tensile stiffness [11]. Since the steady arm holds the contact wire in an inclined direction, and part of its weight is borne by the contact wire, it can be simplified as a mass point-spring model [22] where the lumped mass is the sum of the half mass of the steady arm and the mass of the steady arm clamp, and the spring stiffness is 213 N m^{-1} [11,23]. All the clamps were simplified as lumped mass. The mass of dropper was added on average to the lumped mass of clamp at both ends. Under above simplifications, the dynamic equation of the catenary model can be obtained as follows:

$$\mathbf{M}_c\ddot{\mathbf{z}}_c+\mathbf{C}_c\dot{\mathbf{z}}_c+\mathbf{K}_c\mathbf{z}_c=\mathbf{P}, \tag{1}$$

where $\mathbf{M}_c$, $\mathbf{C}_c$, and $\mathbf{K}_c$ are the mass, damping, and stiffness matrix of the catenary, respectively; $\mathbf{z}_c$ and $\mathbf{P}$ are the displacement and external load vectors of the nodes on the catenary, respectively.

2.2 Dynamic equation of the pantograph

The base of the pantograph is installed on top of the train, and the contact strips on the pan-head contact the contact wire. The dynamic equation of three-mass model of high-speed pantograph is as follows [14,24,25]:

$$\begin{bmatrix} m_3 & 0 & 0 \\ 0 & m_2 & 0 \\ 0 & 0 & m_1 \end{bmatrix}\begin{bmatrix} \ddot{z}_3 \\ \ddot{z}_2 \\ \ddot{z}_1 \end{bmatrix}+\begin{bmatrix} c_3 & -c_3 & 0 \\ -c_3 & c_3+c_2 & -c_2 \\ 0 & -c_2 & c_2+c_1 \end{bmatrix}\begin{bmatrix} \dot{z}_3 \\ \dot{z}_2 \\ \dot{z}_1 \end{bmatrix}$$
$$+\begin{bmatrix} k_3 & -k_3 & 0 \\ -k_3 & k_3+k_2 & -k_2 \\ 0 & -k_2 & k_2+k_1 \end{bmatrix}\begin{bmatrix} z_3 \\ z_2 \\ z_1 \end{bmatrix}=\begin{bmatrix} -F_c \\ F_2 \\ F_1 \end{bmatrix}, \tag{2}$$

where m_i, k_i, c_i, and z_i are the equivalent mass, equivalent stiffness, equivalent damping, and vertical displacement, respectively; subscripts i = 3, 2, 1 represent the pan-head, upper frame, and lower frame, respectively; and F_2 and F_1 are the lifting forces applied to the mass m_2 and m_1, respectively; and F_c is the pantograph-catenary contact force.

2.3 Model of pantograph-catenary interaction

The pantograph and catenary form a coupling dynamic system via the contact force between them. The penalty method can be used to simulate the interaction between the strips and the catenary to solve the contact force between the pantograph and catenary [26,27]:

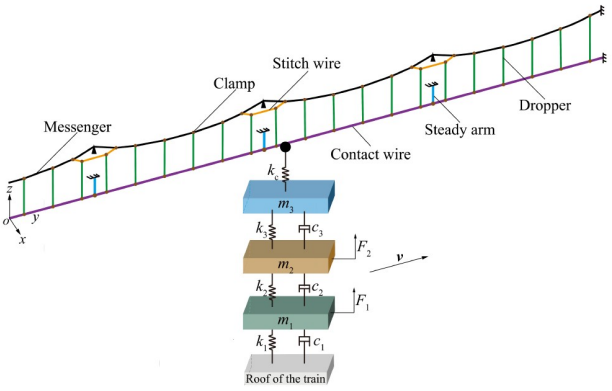

Figure 1 Illustration of the high-speed pantograph-catenary system.

$$F_c=\begin{cases} 0, & z_3-z_c\le 0, \\ k_c(z_3-z_c), & z_3-z_c>0, \end{cases} \tag{3}$$

where z_3 and z_c are the vertical displacements of the pan-head and the contact point of the catenary, respectively. The contact stiffness k_c = 50000 N m^{-1} [28,29].

3. Numerical analysis and verification

3.1 Model of pantograph-catenary interaction

The initial geometric configuration of the catenary was established according to the geometric parameters. The direction along the catenary height H_C was the z-direction, and along the length was the y-direction. The catenary was located on a straight line (z = 0), and the starting point of contact wire was the origin (0, 0). The messenger wire and the stitch wire were on another straight line ($z = H_C$).

Finite element method was used to discretize the structure. In the catenary finite element model, link elements with a length of 0.2 m were used for the contact wire, messenger wire, and stitch wire. Nonlinear spring elements were used for the droppers, and each dropper was divided as one element. Combination of mass element and spring element was used for the steady arm. In the pantograph's three-mass model, mass element and spring element were used for the lumped mass and springs, respectively. In the pantograph-catenary interaction model, Conta175 and Targe169 were used to cover the mass point of the pan-head and the bottom surface of the contact wire, respectively, and the two elements form a contact pair. Full constraints were applied to both ends of the contact wire and messenger wire. A constraint along z-direction was applied to messenger wire support of each span. Full constraint was applied to the end of the steady arm, and only z-directional translational restraint was released on each lumped mass.

Parameters such as elastic modulus, Poisson's ratio,

structural damping, mass and pretension, etc., were assigned to each component. The initial equilibrium state of the catenary was calculated using the negative sag method [30], so that the contact wire can be kept horizontal under the action of gravity and pretension.

From simultaneous Eqs. (1)-(3), the dynamic equilibrium equation of pantograph-catenary system can be obtained as follows:

$$\mathbf{M}\ddot{\mathbf{z}} + \mathbf{C}\dot{\mathbf{z}} + \mathbf{K}\mathbf{z} = \mathbf{F}, \tag{4}$$

where **M**, **C**, and **K** are the mass, damping, and stiffness matrix of the pantograph-catenary system, respectively; **z** and **F** are the displacement and external load vectors of the nodes, respectively. The Newmark method was used for time integration calculation, under the following assumptions:

$$\mathbf{z}_{t+\Delta t} = \mathbf{z}_t + \dot{\mathbf{z}}_t \Delta t + [(0.5-\beta)\ddot{\mathbf{z}}_t + \beta \ddot{\mathbf{z}}_{t+\Delta t}]\Delta t^2, \tag{5}$$

$$\dot{\mathbf{z}}_{t+\Delta t} = \dot{\mathbf{z}}_t + [(1-\alpha)\ddot{\mathbf{z}}_t + \alpha \ddot{\mathbf{z}}_{t+\Delta t}]\Delta t, \tag{6}$$

where $\mathbf{z}_t$ and $\mathbf{z}_{t+\Delta t}$ are the displacement vector at time t and Δt, respectively, and Δt is the time step for integration, $\alpha = 0.5$ and $\beta = 0.25$ are the time integral parameters, respectively.

By combining the simultaneous Eqs. (4)-(6), the dynamic equation pantograph-catenary system can be solved. In the numerical calculation, the maximum integration step of time was 0.00167 s, the interval time for output was 0.005 s, and the initial position of the pantograph was $y = 0$. To determine the lifting forces F_2 and F_1 applied to mass elements m_2 and m_1, respectively, dynamic calculation and iteration were conducted until the mean of contact force reached the target value. After that, the contact force, lifting displacements, etc., in the pantograph-catenary system were calculated. The simulation calculation was implemented by the commercial software ANSYS. The pantograph-catenary interaction model established in this section has been verified by the reference model results in EN50318:2018 [10].

3.2 Verification by measured data from line tests

Based on 16 sets of measured data of DSA380 high-speed pantograph operating on the Yangquxi-Yuanpingxi section of the Datong-Xi'an High-speed Railway Line, the statistics of the measured data, such as mean value F_m, standard deviation σ, statistical maximum $F'_{max} = F_m + 3\sigma$, statistical minimum $F'_{min} = F_m - 3\sigma$ of contact force, and the range of vertical position of the contact point (RVPCP), at running speed of 0-360 km h^{-1} are obtained (hollow discrete points in Fig. 2). Least square method was used to fit the measured data with a fourth-degree polynomial, and the fitting curves obtained represent the measured values of the line tests at different running speeds (solid lines in Fig. 2a-c). In particular, when the running speeds are 350 km h^{-1}, 300 km h^{-1}, and 250 km h^{-1}, the line test values of F_m are 192.39 N, 157.67 N, and 132.71 N, respectively, and their relative deviations from the empirical values $0.00097v + 70$ [3] (chain-dotted line in Fig. 2a) are less than 1.9%. The measured data of F_m would be used to determine the calculation parameters of the pantograph-catenary dynamics model.

The pantograph-catenary dynamic model established in Sect. 2.1 was used to calculate the dynamic behavior of DSA380 pantograph operating on the Datong-Xi'an High-speed Railway Line. The span of the catenary was 55 m. The models of the contact wire, messenger wire, stitch wire, and dropper were CTMH150, JTMH120, JTMH35, and JTMH10, respectively. The pre-tensions of the contact wire, messenger wire, and stitch wire were 30 kN, 21 kN, and 3.5 kN, respectively. For the DSA380 pantograph with a working height of 1600 mm, the equivalent masses of the pan-head, upper frame, and lower frame were 7.94 kg, 8.22 kg, and 5.90 kg, respectively; their equivalent stiffnesses were 6650 N m^{-1}, 13181 N m^{-1}, and 74.0 N m^{-1}, respectively; and the equivalent damping were 85.31 N s m^{-1}, 11.90 N s m^{-1}, and 67.41 N s m^{-1}, respectively.

In the finite element simulation, the span number of the catenary was 30. Iterative calculation was carried out until the mean values of the contact force at various running speeds reached the measured values from line tests. When the running speeds were 350 km h^{-1}, 300 km h^{-1}, and 250 km h^{-1}, the obtained static contact forces were 83.85 N, 76.06 N, and 78.42 N, respectively, and the curves of the contact force and vertical displacement of the contact point (VDCP) versus time were shown as thick solid lines in Fig. 3a-c. After that, the data of the 10th-20th spans were statistically analyzed. It can be seen that the probability distribution of the contact force basically conforms to a normal distribution, that is, the probability that the contact force of the pantograph-catenary lies in the interval $[F_{max}, F_{min}]$ is 99.74%. On the one hand, the deviations of the calculated F_m, σ, and the RVPCP (solid dots in Fig. 2a-c) from the measured values are within the tolerances given in EN50318:2018 [4] (dashed lines in Fig. 2a-c). When the running speeds are 350 km h^{-1}, 300 km h^{-1}, and 250 km h^{-1}, the deviations of F_m are 0.16 N, –1.23 N, and 1.24 N, respectively, all within the allowable tolerances of ± 2.5 N (Fig. 2a); the deviations of σ are 2.65 N, 1.98 N, and –4.53 N, respectively, all within the given tolerances of ± 20% (Fig. 2b); the deviations of RVPCP are –5.2 mm, –5.6 mm, and –8.7 mm, respectively, within the given tolerances of ± 20 mm (Fig. 2c). On the other hand, the F'_{max} and F'_{min} obtained by simulation are located at the upper and lower bounds of the measured values, that is, they represent the two extreme behaviors of the pantograph-catenary system (Fig. 2d). Therefore, the dynamic modeling and simulation results of the high-speed pantograph-catenary system in this article are in good match with the measured data from line tests of the DSA380 on the Datong-Xi'an High-speed Railway Line.

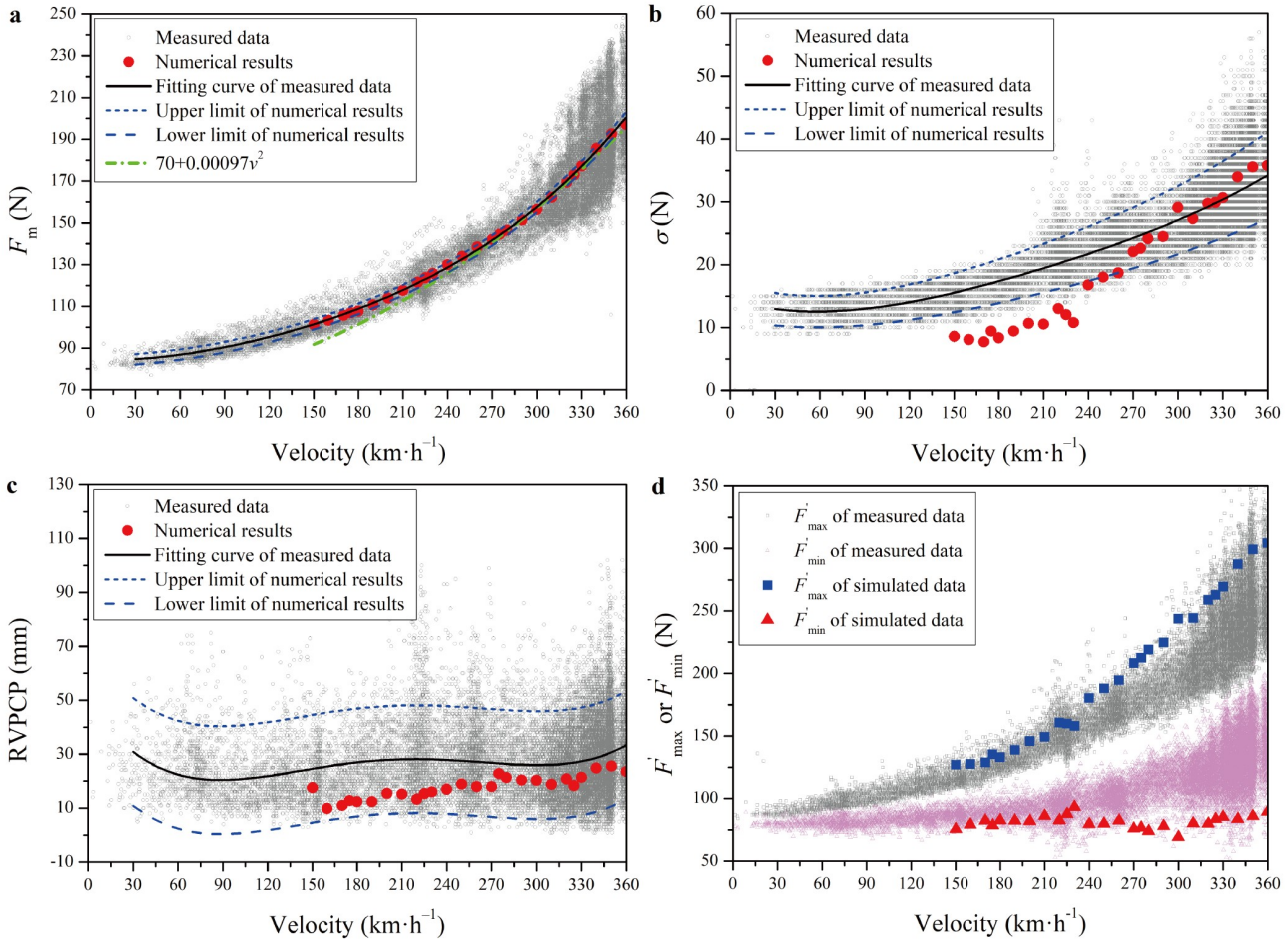

Figure 2 Verification by measured data from line tests. **a** F_m; **b** σ; **c** RVPCP; **d** F'_{max} and F'_{min}.

Furthermore, using the time history curves and the relevant statistical information in the case of 30 spans, and considering calculation precision, calculation time, and initial transient and end effects, the numerical parameters are determined as follows: for running speeds of 350 km h^{-1}, 300 km h^{-1}, and 250 km h^{-1}, the catenary span numbers are 20, 20, and 17, respectively, and the analysis sections are 10th-16th span, 10th-15th span, and 8th-12th span, respectively. Comparing the 20 or 17-span catenary with the 30-span catenary, the time history curves shown in fine lines in Fig. 3a-c almost completely overlap, with differences in contact force standard deviations less than 0.2 N and relative deviations about 1.0%. Therefore, the reduced catenary span numbers and analysis sections will be used for the pantograph parameter optimization calculation.

4. Parameter optimization of three-mass model of pantograph

4.1 Description

Figure 4 shows $\Delta\sigma$, the changes of the standard deviation of the contact force when each model parameter of DSA380 pantograph varies by ± 1% individually at various speeds. It can be seen that, when the equivalent mass of the pan-head, m_3, decreases, $\Delta\sigma$ is negative, and vice versa. In addition, $\Delta\sigma$ caused by increase or decrease of m_3 is three times higher than that of the other parameters. These results are coincident with the existing reports [8,11-13]. Therefore, reduction of m_3 may effectively reduce the fluctuation of the contact force, and its influence weight on the standard deviation of contact force is much higher than the other parameters.

DSA380 is a classical double-strip high-speed pantograph with the equivalent mass of pan-head m_3 = 7.94 kg. The decision vector $\mathbf{X} = [m_2, m_1, k_3, k_2, k_1, c_3, c_2, c_1]^T$, that is, eight parameters of the three-mass model, was optimized except m_3, to reduce the fluctuation intensity of the contact force of the pantograph-catenary system. And the objective function was the standard deviation of the contact force in the frequency range of 0-20 Hz. The goal of optimization was to minimize of the objective function. The constraints of the eight design variables in the decision vector **X** were determined in consideration of the engineering design possibility. In addition, during the process of optimization, the static contact force coincided to that of the measured data at the same running speed. Therefore, the optimization problem

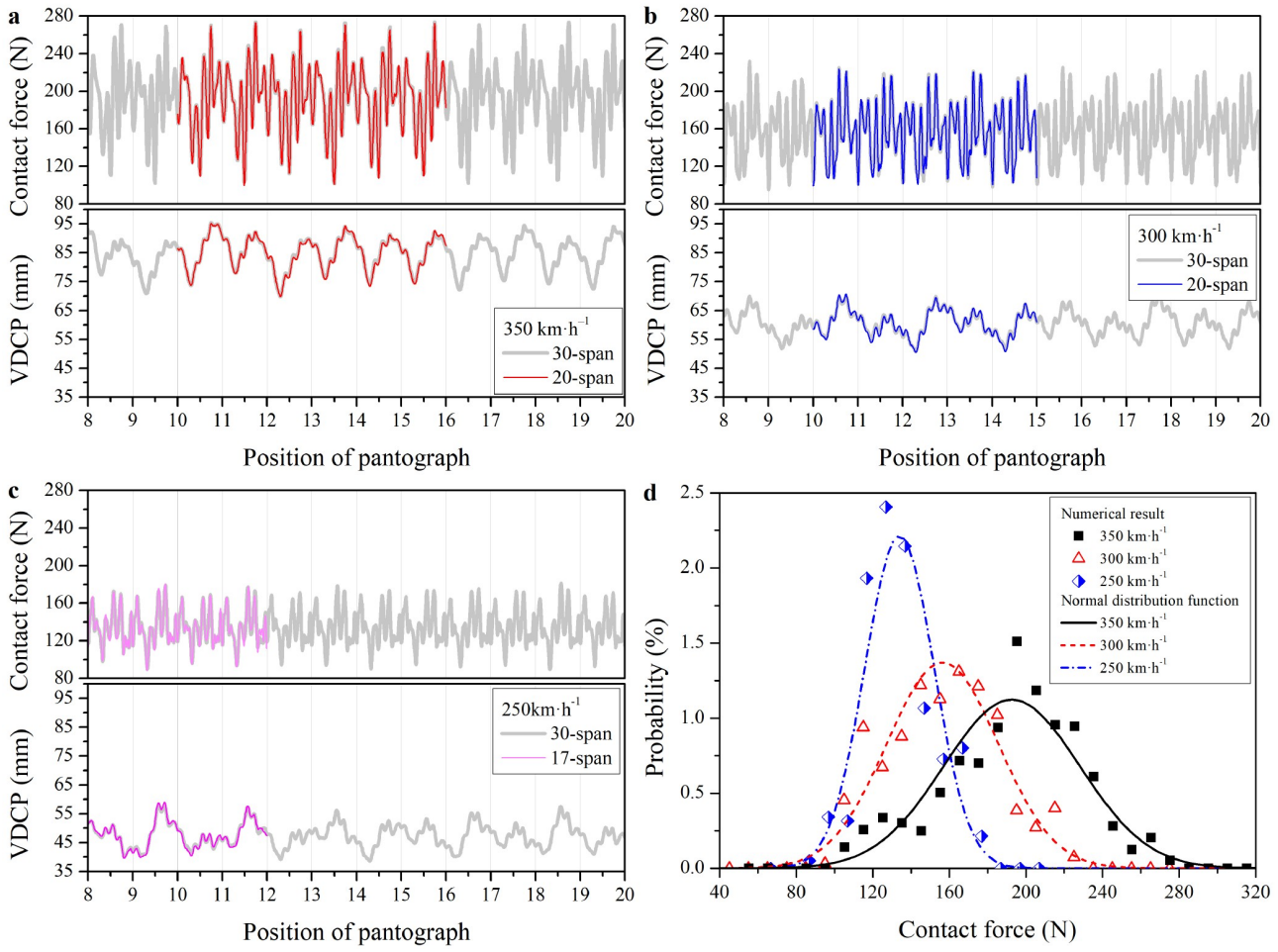

Figure 3 Time history curves of contact force (after 20 Hz low pass filtering) and VDCP when the speeds are **a** 350 km h^{-1}; **b** 300 km h^{-1}; **c** 250 km h^{-1}, respectively; **d** probability distribution of contact force.

can be described as follows:

$$\min\sigma(\mathbf{X})$$

$$\mathbf{X} = [m_2, m_1, k_3, k_2, k_1, c_3, c_2, c_1]^{\mathrm{T}},$$

$$\text{s.t.}\begin{cases} m_2 \in [5\ \text{kg}, 20\ \text{kg}], \\ m_1 \in [3\ \text{kg}, 20\ \text{kg}], \\ k_3 \in [4000\ \text{N m}^{-1}, 14000\ \text{N m}^{-1}], \\ k_2 \in [8000\ \text{N m}^{-1}, 20000\ \text{N m}^{-1}], \\ k_1 \in [0\ \text{N m}^{-1}, 200\ \text{N m}^{-1}], \\ c_3 \in [0\ \text{N s m}^{-1}, 100\ \text{N s m}^{-1}], \\ c_2 \in [0\ \text{N s m}^{-1}, 50\ \text{N s m}^{-1}], \\ c_3 \in [10\ \text{N s m}^{-1}, 240\ \text{N s m}^{-1}]. \end{cases}$$

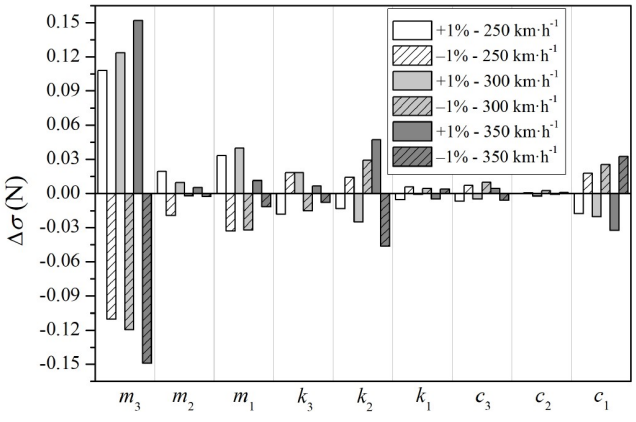

Figure 4 Changes of the standard deviation of contact force when each model parameter of DSA380 varies by ± 1% individually at various speeds.

4.2 Parameter optimization process

In order to search for the global optimum solution in a highly efficient way, the genetic algorithm method [31,32] combined with the basic descent method [33] was adopted to carry out joint optimization of the eight dynamic parameters. In calculation, the final number of iterations for the genetic algorithm was first set, and the iteration results of the decision vector obtained from the genetic algorithm were then used as the starting point of the basic descent algorithm, to obtain the final optimum solution.

The detailed procedures are as follows:

Using Gray code [34], divide the domains of m_2, m_1, k_3, k_2, and k_1 into 15 segments, respectively, and divide the domains of c_3, c_2, and c_1 into 7 segments, respectively. There are 2^{29} parameter combinations in the whole parameter space. Each parameter combination is called a decision vector, which is represented by the symbol of $\mathbf{X}$.

Using the genetic algorithm, perform decision vector iteration in the whole parameter space, with minimum standard deviation of the contact force as the target. The number of the decision vectors in each generation population is 100, and the number of iterations is 20.

Randomly generate 100 decision vectors to form the first-generation population. For each decision vector, perform the dynamic calculation based on the dynamic model of pantograph-catenary system based on Sect. 2.1 to obtain the contact force standard deviation σ. The smaller the σ is, the higher the fitness value of the decision vector is.

Based on the decision vectors of the $(i-1)$th (i = 2, 3, …, 21) generation population, treat the decision vector with selection operator, crossover operator and mutation operator successively, to produce the decision vectors of the ith generation population.

Note the decision vector with the minimum σ in the 20th generation population as $\mathbf{X}^0$. For convenience, note the $\mathbf{X}^0$ at 350 km h^{-1}, 300 km h^{-1}, and 250 km h^{-1} as $\mathbf{X}^0_{350}$, $\mathbf{X}^0_{300}$, and $\mathbf{X}^0_{250}$, respectively. The change tendency of σ corresponding to each generation of population with the generation number is shown in Fig. 5, where each discrete point represents a specific decision vector. By successively connecting the minimum σ of each generation population with lines, curves showing the variation of the population optimum value with the generation number are obtained. It can be seen that as the generation number increases, both the population optimum value and its descent rate gradually decreases.

Take $\mathbf{X}^0$ as the starting point, perform iteration to find the global optimal solutions $\mathbf{X}^*_{350}$, $\mathbf{X}^*_{300}$, and $\mathbf{X}^*_{250}$ at 350 km h^{-1}, 300 km h^{-1}, and 250 km h^{-1}, respectively, by the basic descent method.

5. Results

5.1 Optimum solutions at various running speeds

At the running speeds of 350 km h^{-1}, 300 km h^{-1}, and 250 km h^{-1}, and with minimum standard deviation of the contact force as the target, joint optimization among eight parameters except the equivalent mass of the pan-head was performed to obtain the optimum solutions $\mathbf{X}^*_{350}$, $\mathbf{X}^*_{300}$, and $\mathbf{X}^*_{250}$ of the three-mass model of the pantograph. In detail, $\mathbf{X}^*_{350}$ = [8.00 kg, 3.00 kg, 14000 N m^{-1}, 8000 N m^{-1}, 200 N m^{-1}, 0.00 N s m^{-1}, 28.57 N s m^{-1}, 240.00 N s m^{-1}]$^{\mathrm{T}}$, $\mathbf{X}^*_{300}$ = [13.00 kg, 17.73 kg, 13333 N m^{-1}, 8000 N m^{-1}, 200 N m^{-1}, 14.29 N s m^{-1}, 42.86 N s m^{-1}, 240.00 N s m^{-1}]$^{\mathrm{T}}$,

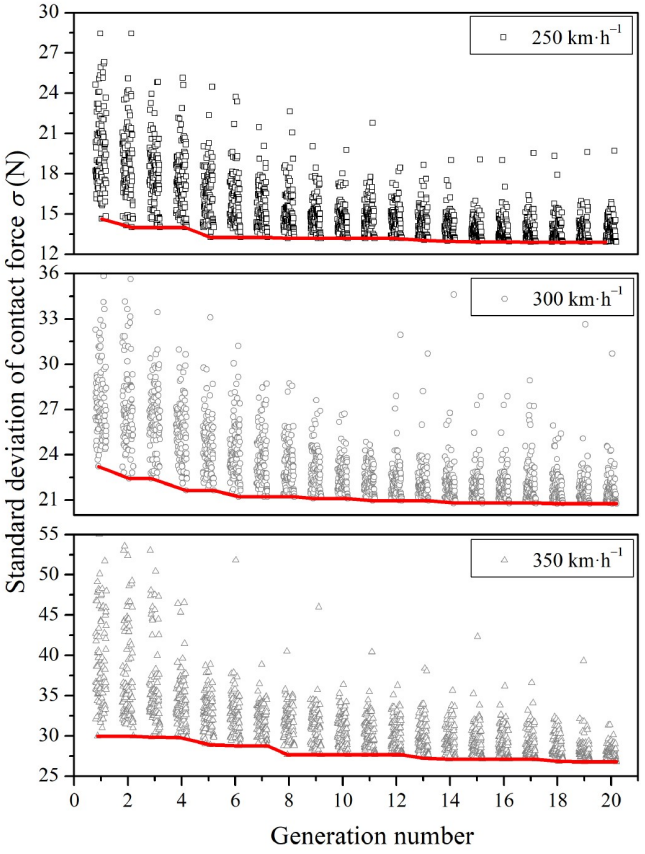

Figure 5 Change tendency of the standard deviation of contact force.

$\mathbf{X}^*_{250}$ = [5.00 kg, 3.00 kg, 10000 N m^{-1}, 20000 N m^{-1}, 200 N m^{-1}, 0.00 N s m^{-1}, 0.00 N s m^{-1}, 141.43 N s m^{-1}]$^{\mathrm{T}}$ (Table 1). Among them, the optimum equivalent stiffness of the lower frame, k_1, was all 200 N m^{-1}, while the optimum solutions of other seven parameters were related to the running speeds. Therefore, it is necessary to design the equivalent parameters in terms of the range of the running speed during the pantograph in normal service to achieve the optimal matching of the pantograph-catenary parameters.

The time history curves of the contact force and VDCP corresponding to optimal solutions $\mathbf{X}^*_{350}$, $\mathbf{X}^*_{300}$, and $\mathbf{X}^*_{250}$ (hollow symbols in Fig. 6) have the same fluctuation tendency as those of the DSA380 (thick solid lines in Fig. 6), while the oscillation amplitudes are significantly reduced, and their standard deviations of the contact force, σ, are 26.21 N, 20.35 N, and 12.76 N, respectively (Table 2). Correspondingly, σ of the DSA380 at the speeds of 350 km h^{-1}, 300 km h^{-1}, and 250 km h^{-1} are 35.72 N, 28.94 N, and 18.17 N, respectively, which indicating that eight-parameter joint optimizations reduced σ by 26.6%, 29.7%, and 29.8%, respectively. The effects of eight-parameter joint optimization are significantly higher than the results of single-parameter optimization of the eight parameters except the equivalent mass of the pan-head and dual-parameter optimization of the equivalent stiffness and

Table 1 Optimal solutions and model parameters of DSA380

	Equivalent mass (kg)		Equivalent stiffness (N m^{-1})			Equivalent damping (N s m^{-1})		
	m_2	m_1	k_3	k_2	k_1	c_3	c_2	c_1
$\mathbf{X}_{\mathrm{DSA380}}$	8.22	5.90	6650	13181	74	85.31	11.90	67.41
$\mathbf{X}^*_{350}$	8.00	3.00	14000	8000	200	0.00	28.57	240.00
$\mathbf{X}^*_{300}$	13.00	17.73	13333	8000	200	14.29	42.86	240.00
$\mathbf{X}^*_{250}$	5.00	3.00	10000	20000	200	0.00	0.00	141.43
$\mathbf{X}^*_{\mathrm{DSA380}}$	8.22	3.00	14000	8000	200	0.00	11.90	240.00

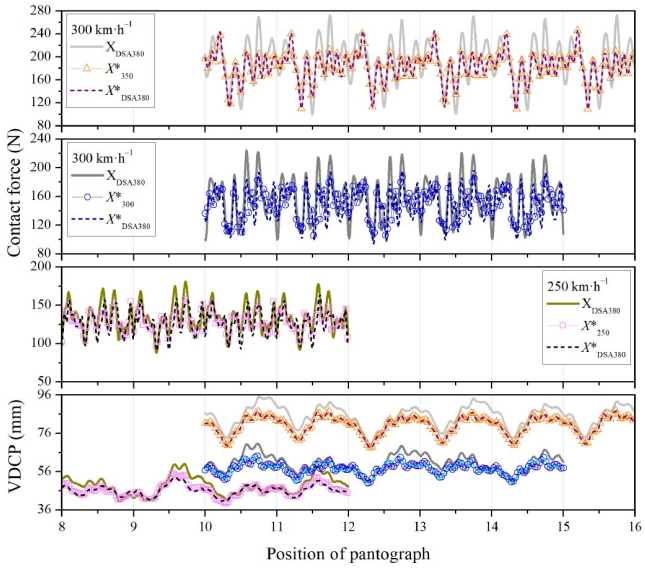

Figure 6 Time history curves of the contact force (after 20 Hz low pass filtering) and VDCP.

Table 2 Standard deviation of contact force of the optimal solutions and the relative deviation from that of DSA380[a)]

Running speed (km h^{-1})	Standard deviation of contact force (N)			Relative deviation (%)	
	DSA380	$\mathbf{X}^*_i$	$\mathbf{X}^*_{\mathrm{DSA380}}$	$\mathbf{X}^*_i$	$\mathbf{X}^*_{\mathrm{DSA380}}$
350	35.72	26.21	26.27	−26.6	−26.5
300	28.94	20.35	22.70	−29.7	−21.6
250	18.17	12.76	15.53	−29.8	−14.5

a) The subscript i in $\mathbf{X}^*_i$ represents the running speed

damping of the pan-head [10]. At the running speed of 350 km h^{-1}, the standard deviations of the contact force are declined by 3.13 N and 1.58 N, respectively.

5.2 Proposed optimization for the DSA380 high-speed pantograph

During the operation of the pantograph, it is unrealistic to adjust all pantograph parameters in real time according to the changing running speed. Comprehensively considering DSA380 mainly serving in high-speed railway sections, the difference between DSA380's existing service parameters and the optimum solutions of double-strip pantograph at various running speeds, and the sensitivity analysis around the optimization solutions, an optimization scheme $\mathbf{X}^*_{\mathrm{DSA380}}$ for DSA380 high-speed pantograph was proposed (Table 1 and Fig. 7).

Though the optimum solutions of the equivalent damping of the upper frame, c_2, at different speeds have relatively large differences, when c_2 changes from the optimum solution to the present value of DSA380, 11.90 N s m^{-1}, the percentage increases in σ are only 0.04%, 0.44%, and 0.00%, respectively, corresponding to 350 km h^{-1}, 300 km h^{-1}, and 250 km h^{-1}, indicating almost unchanged σ (Fig. 7g), so c_2 = 11.90 N s m^{-1} is suggested. When the equivalent damping of the pan-head, c_3, decreases from the optimal solution at 300 km h^{-1}, 14.29 N s m^{-1}, to the optimal value at both 350 km h^{-1} and 250 km h^{-1}, 0 N s m^{-1}, σ only increases by 0.34% (Fig. 7f), so c_3 = 0 N s m^{-1} is suggested. When the equivalent mass of the lower frame, m_1, reduces from the optimal solution at 300 km h^{-1}, 17.73 kg, to the optimal value at both 350 km h^{-1} and 250 km h^{-1}, 3.00 kg, σ only increases by 4.18% (Fig. 7b), so m_1 = 3.00 kg is suggested. When the equivalent damping of the lower frame, c_1, increases from the optimum value at 250 km h^{-1}, 141.43 N s m^{-1}, to the optimal value at both 350 km h^{-1} and 300 km h^{-1}, 240.00 N s m^{-1}, σ increases by only 5.33% (Fig. 7h), so c_1 = 240.00 N s m^{-1} is suggested. When the equivalent stiffness of pan-head, k_3, increases from the optimum

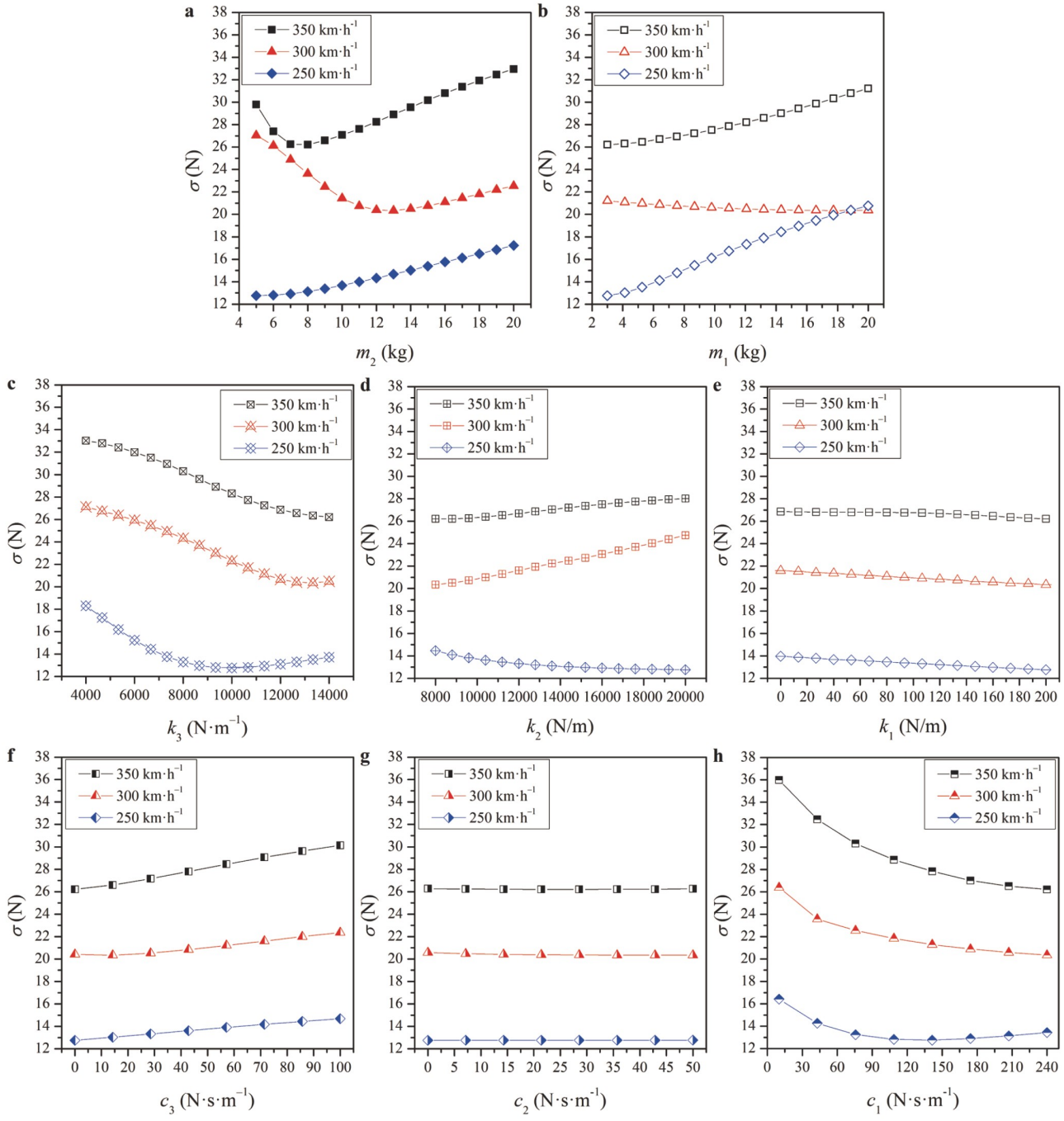

Figure 7 Sensitivity analysis at the optimal solutions of different speeds. **a** m_2; **b** m_1; **c** k_3; **d** k_2; **e** k_1; **f** c_3; **g** c_2; **h** c_1.

values at 300 km h^{-1} and 250 km h^{-1}, 13333 N m^{-1} and 10000 N m^{-1}, respectively, to the optimum value at 350 km h^{-1}, 14000 N m^{-1}, σ increases by only 0.64% and 7.60%, respectively (Fig. 7c), so k_3 = 14000 N m^{-1} is suggested. When the equivalent stiffness of the upper frame, k_2, decreases from the optimum value at 250 km h^{-1}, 20000 N m^{-1}, to the optimum value at 350 km h^{-1} and 300 km h^{-1}, 8000 N m^{-1}, σ increases by 1.69 N, with an increased percentage of 13.24% (Fig. 7d), so k_2 = 8000 N m^{-1} is suggested. The optimum values of the equivalent mass of the upper frame, m_2, at different speeds have relatively large differences, when m_2 changes from its optimum values to the present value of DSA380, 8.22 kg, σ increases by 0.23%, 14.94%, and 3.21%, respectively, corresponding to 350 km h^{-1}, 300 km h^{-1}, and 250 km h^{-1} (Fig. 7a), so m_2 = 8.22 kg is suggested.

In summary, the recommended optimal scheme for DSA380 high-speed pantograph is $\mathbf{X}^*_{\mathrm{DSA380}}$ = [8.22 kg, 3.00 kg, 14000 N m^{-1}, 8000 N m^{-1}, 200 N m^{-1}, 0.00 N s m^{-1}, 11.90 N s m^{-1}, 240.00 N s m^{-1}]$^{\mathrm{T}}$ (Table 1),

where the mean contact forces, F_m, at 350 km h^{-1}, 300 km h^{-1}, and 250 km h^{-1} are 182.69 N, 149.33 N, and 128.38 N, respectively, satisfying the requirement of $F_m > 0.00047v^2 + 60$ in EN30367:2012 [3]. Comparing to DSA380, the standard deviations of the contact force decrease by –9.45 N, 6.24 N, and 2.64 N, respectively, and their relative deviation are about 26.5%, 21.6%, and 14.5%, respectively (Table 2); the maximum contact forces, F_{max}, decrease by 26.14 N, 27.14 N, and 16.55 N, respectively; the minimum contact forces, F_{min}, increase by 8.74 N, –5.14 N, and 2.60 N. After using the parameters of $\mathbf{X}^*_{DSA380}$ for the pantograph, F_m, σ, and F_{max} reduce remarkably. The reduction of F_m will decrease the friction between the contact strips and wires, the reduction of σ will decrease the intensity of fluctuation of the contact force, and the reduction of F_{max} will lower the event probability of straddling, and reduce the friction between the contact parts. Moreover, F_{min} becomes larger except at 300 km h^{-1}, which can reduce the loss of contact probability, while F_{min} is 93.77 N at 300 km h^{-1} which is much larger than 0 N at which off-line events will happen. Compared with the present parameters of DSA380, the pantograph-catenary coupling quality of $\mathbf{X}^*_{DSA380}$ at different speeds is significantly improved.

6. Conclusions

Based on the experimentally measured three-mass model parameters of DSA380, a typical double-strip high-speed pantograph in service at a working height of 1600 mm, and the catenary parameters of Datong-Xi'an High-speed Railway Line, a two-dimensional dynamics model for stitched catenary system and three-mass model of pantograph was established, which was verified not only by the reference model in EN50318:2018 [4,10], but also by the measured data. The changes of standard deviation of the contact force with each three-mass model parameter of DSA380 changes ± 1% were calculated by the pantograph-catenary dynamic simulation. It can be seen that the equivalent mass of the pan-head had a much higher impact on the pantograph-catenary coupling quality than other eight parameters.

Using the genetic algorithm and basic descent method, and taking the standard deviation of the contact force as the optimization target, an eight-parameter joint optimization scheme for double-strip high-speed pantograph at different running speeds was present. The results indicated that, the optimization scheme and effect are closely related to the running speed and that the effect is much better than that of single-parameter or dual-parameter optimization. As compared with DSA380 at the running speeds of 350 km h^{-1}, 300 km h^{-1}, and 250 km h^{-1}, the standard deviation of the contact force decreased by 26.6%, 29.7%, and 29.8%, respectively. This result can provide some guidance for parameter design of new model high-speed pantograph with two contact strips.

Combining the sensitivity analysis at the optimal solutions and the parameters and characteristics in service of DSA380, an optimization scheme for DSA380 was introduced, that is, reducing the equivalent damping of the pan-head to 0 N s m^{-1}, increasing the equivalent stiffness of pan-head to 14000 N m^{-1}, reducing the equivalent stiffness of upper frame to 8000 N m^{-1}, keeping the equivalent mass and damping of the upper frame unchanged, increasing the equivalent damping of lower frame to 240 N s m^{-1}, increasing the equivalent stiffness of lower frame to 200 N m^{-1}, and reducing the equivalent mass of lower frame to 3 kg. At the running speeds of 350 km h^{-1}, 300 km h^{-1}, and 250 km h^{-1}, this optimization scheme reduced the standard deviation of the contact force by 26.5%, 21.6%, and 14.5%, respectively, compared with the present DSA380. It provides a reference for the parameter optimization of the in-service models of high-speed pantographs.

This work was supported by the National Natural Science Foundation of China (Grant No. 11672297), and the Strategic Priority Research Program of the Chinese Academy of Sciences (Grant No. XDB22020200).

1 G. W. Yang, Y. J. Wei, G. L. Zhao, Y. Liu, X. H. Zeng, Y. L. Xing, J. Lai, Y. Y. Zhang, H. Wu, Q. Chen, Q. S. Liu, J. C. Li, K. X. Hu, Z. P. Yang, W. Z. Liu, W. J. Wang, S. G. Sun, W. H. Zhang, N. Zhou, R. P. Li, Q. S. Lv, X. S. Jin, Z. F. Wen, X. B. Xiao, X. Zhao, D. B. Cui, B. Wu, S. Q. Zhong, and X. Zhou, Research progress on the mechanics of high speed rails (in Chinese), Adv. Mech. **45**, 217 (2015).

2 EN 50317:2012, Railway applications-current collection systems-requirements for and validation of measurements of the dynamic interaction between pantograph and overhead contact line (2012).

3 EN 50367:2012, Railway applications-current collection systems-technical criteria for the interaction between pantograph and overhead line (to achieve free access) (2012).

4 EN 50318:2018, Railway applications-current collection systems-validation of simulation of the dynamic interaction between pantograph and overhead contact line (2018).

5 Y. H. Cho, K. Lee, Y. Park, B. Kang, and K. Kim, Influence of contact wire pre-sag on the dynamics of pantograph-railway catenary, Int. J. Mech. Sci. **52**, 1471 (2010).

6 S. Gregori, M. Tur, E. Nadal, and F. J. Fuenmayor, An approach to geometric optimisation of railway catenaries, Vehicle Syst. Dyn. **56**, 1162 (2018).

7 J. Zhang, W. Liu, and Z. Zhang, Sensitivity analysis and research on optimisation methods of design parameters of high-speed railway catenary, IET Electr. Syst. Transp. **9**, 150 (2019).

8 J. Pombo, and J. Ambrósio, Influence of pantograph suspension characteristics on the contact quality with the catenary for high speed trains, Comput. Struct. **110-111**, 32 (2012).

9 N. Zhou, and W. Zhang, Investigation on dynamic performance and parameter optimization design of pantograph and catenary system, Finite Elem. Anal. Des. **47**, 288 (2011).

10 M. Z. Wu, Y. Liu, and X. H. Xu, Sensitivity analysis and optimization on parameters of high speed pantograph-catenary system (in Chinese), Chin. J. Theo. Appl. Mech. **53**, 75 (2021).

11 J. H. Lee, Y. G. Kim, J. S. Paik, and T. W. Park, Performance evaluation and design optimization using differential evolutionary algorithm of the pantograph for the high-speed train, J. Mech. Sci. Technol. **26**, 3253 (2012).

12 J. Ambrósio, J. Pombo, and M. Pereira, Optimization of high-speed railway pantographs for improving pantograph-catenary contact, Theor. Appl. Mech. Lett. **3**, 013006 (2013).
13 X. Y. Wang, X. H. Nian, X. Y. Chu, and P. Yue, in Research on dynamic performance and parameter optimization of the high-speed pantograph and catenary system: Proceedings of the 8th IEEE Prognostics and System Health Management Conference, Harbin, 2017.
14 A. Collina, and S. Bruni, Numerical simulation of pantograph-overhead equipment interaction, Vehicle Syst. Dyn. **38**, 261 (2002).
15 S. Bruni, J. Ambrosio, A. Carnicero, Y. H. Cho, L. Finner, M. Ikeda, S. Y. Kwon, J. P. Massat, S. Stichel, M. Tur, and W. Zhang, The results of the pantograph-catenary interaction benchmark, Vehicle Syst. Dyn. **53**, 412 (2015).
16 D. Zou, N. Zhou, L. Rui Ping, G. M. Mei, and W. H. Zhang, Experimental and simulation study of wave motion upon railway overhead wire systems, Proc. Inst. Mech. Eng. Part F-J. Rail Rapid Transit **231**, 934 (2017).
17 G. Poetsch, J. Evans, R. Meisinger, W. Kortüm, W. Baldauf, A. Veitl, and J. Wallaschek, Pantograph/catenary dynamics and control, Vehicle Syst. Dyn. **28**, 159 (1997).
18 G. Gilbert, and H. E. H. Davies, Pantograph motion on a nearly uniform railway overhead line, Proc. Inst. Electr. Eng. UK **113**, 485 (1966).
19 P. R. Scott, and M. Rothman, Computer evaluation of overhead equipment for electric railroad traction, IEEE Trans. Ind. Applicat. **IA-10**, 573 (1974).
20 Y. Song, Z. Liu, F. Duan, Z. Xu, and X. Lu, Wave propagation analysis in high-speed railway catenary system subjected to a moving pantograph, Appl. Math. Model. **59**, 20 (2018).
21 Y. Song, P. Antunes, J. Pombo, and Z. Liu, A methodology to study high-speed pantograph-catenary interaction with realistic contact wire irregularities, Mech. Mach. Theor. **152**, 103940 (2020).
22 F. Vesali, H. Molatefi, M. A. Rezvani, B. Moaveni, and M. Hecht, New control approaches to improve contact quality in the conventional spans and overlap section in a high-speed catenary system, Proc. Inst. Mech. Eng. Part F-J. Rail Rapid Transit **233**, 988 (2019).
23 Y. H. Cho, Numerical simulation of the dynamic responses of railway overhead contact lines to a moving pantograph, considering a nonlinear dropper, J. Sound Vib. **315**, 433 (2008).
24 S. D. Eppinger, D. N. O'Connor, W. P. Seering, and D. N. Wormley, Modeling and experimental evaluation of asymmetric pantograph dynamics, J. Dyn. Syst. Measure. Control **110**, 168 (1988).
25 R. M. G. A. Vieira, High speed train pantograph models identification, Dissertation for the Master's Degree (Technical University of Lisbon, Lisbon, 2016).
26 R. D. Cook, Finite element modeling for stress analysis (John Wiley & Sons, Madison, 1995).
27 Y. Zhang, L. Wang, H. Zhao, and S. T. Lie, Extraction of mode shapes of beam-like structures from the dynamic response of a moving mass, Acta Mech. Sin. **35**, 664 (2019).
28 EN 50318:2002, Railway applications-current collection systems-validation of simulation of the dynamic interaction between pantograph and overhead contact line (2002).
29 P. Antunes, J. Ambrósio, J. Pombo, and A. Facchinetti, A new methodology to study the pantograph–catenary dynamics in curved railway tracks, Veh. Syst. Dyn. **58**, 425 (2020).
30 N. Zhou, R. P. Li, and W. H. Zhang, Modeling and simulation of catenary based on negative sag method (in Chinese), J. Traffic Transport. Eng. **9**, 28 (2009).
31 J. H. Holland, Adaptation in Natural and Artificial Systems (MIT Press, Cambridge, 1992).
32 D. E. Goldberg, Genetic Algorithms in Search, Optimization, and Machine Learning (Pearson Education, Patparganj, 2006).
33 G. D. Cheng, Introduction to optimum design of engineering structures (in Chinese) (Dalian University of Technology Press, Dalian, 2012).
34 R. A. Caruana, and J. D. Schaffer, in Representation and hidden bias: gray vs. binary coding for genetic algorithms: Proceedings of the Fifth International Conference on Machine Learning, Ann Arbor, 12 June-14 June, 1988 (University of Michigan, Ann Arbor, 1988).

双滑板高速受电弓的多参数联合优化以提高弓网耦合质量

吴孟臻, 许向红, 燕永钊, 罗羿, 黄思俊, 王建山

摘要 高速列车的大幅提速, 将导致弓网动态接触力振荡更加剧烈, 给弓网关系研究和高速受电弓设计提出了挑战. 良好的弓网耦合质量是确保高速列车安全高效运行、稳定可靠受流、降低接触线与受电弓滑板磨耗等的基本前提. 其中, 高速受电弓的动力学参数对弓网耦合质量至关重要. 本文以降低弓网接触力标准差为优化目标, 提出了多个运行速度下的双滑板高速受电弓的多参数联合优化设计方案. 此外, 结合最优解处的敏度分析, 以及DSA380型双滑板高速受电弓的现役参数和服役特点, 给出了DSA380的优化建议.